Experimental Testing and Validation of Selected Tools for Mooring Analysis

M5, T4.1 & T4.2

Thomsen, Jonas Bjerg; Ferri, Francesco; Kofoed, Jens Peter

Publication date:
2018

Document Version
Publisher's PDF, also known as Version of record

DEPARTMENT OF CIVIL ENGINEERING
AALBORG UNIVERSITY

Experimental Testing and Validation of Selected Tools for Mooring Analysis

M5, T4.1 & T4.2

Jonas Bjerg Thomsen
Francesco Ferri
Jens Peter Kofoed

ISSN 1901-726X
DCE Technical Report No. 245

Aalborg University
Department of Civil Engineering
Wave Energy Research Group

DCE Technical Report No. 245

Experimental Testing and Validation of Selected Tools for Mooring Analysis

M5, T4.1 & T4.2

by

Jonas Bjerg Thomsen
Francesco Ferri
Jens Peter Kofoed

June 2018

Scientific Publications at the Department of Civil Engineering

Technical Reports are published for timely dissemination of research results and scientific work carried out at the Department of Civil Engineering (DCE) at Aalborg University. This medium allows publication of more detailed explanations and results than typically allowed in scientific journals.

Technical Memoranda are produced to enable the preliminary dissemination of scientific work by the personnel of the DCE where such release is deemed to be appropriate. Documents of this kind may be incomplete or temporary versions of papers—or part of continuing work. This should be kept in mind when references are given to publications of this kind.

Contract Reports are produced to report scientific work carried out under contract. Publications of this kind contain confidential matter and are reserved for the sponsors and the DCE. Therefore, Contract Reports are generally not available for public circulation.

Lecture Notes contain material produced by the lecturers at the DCE for educational purposes. This may be scientific notes, lecture books, example problems or manuals for laboratory work, or computer programs developed at the DCE.

Theses are monograms or collections of papers published to report the scientific work carried out at the DCE to obtain a degree as either PhD or Doctor of Technology. The thesis is publicly available after the defence of the degree.

Latest News is published to enable rapid communication of information about scientific work carried out at the DCE. This includes the status of research projects, developments in the laboratories, information about collaborative work and recent research results.

Published 2018 by
Aalborg University
Department of Civil Engineering
Thomas Manns Vej 23
DK-9220 Aalborg Ø, Denmark

Printed in Aalborg at Aalborg University

ISSN 1901-726X
DCE Technical Report No. 245

Preface

This report covers a description of an experimental test campaign conducted at Aalborg University as part of the project *"Mooring Solutions for Large Wave Energy Converters"*. Furthermore, the test data is used to validate numerical tools to be used in initial design of mooring solutions for large floating WECs. The validation considers both a quasi-static using a self-develop script and a full dynamic approach using the commercial software package OrcaFlex.

The report is the outcome of Work Package 4, Task 4.1 and 4.2 of the project. Thereby, the report forms the *"Milestone 5: Report on validation/calibration of analysis tool"*. The report has been produced by Aalborg University with input from Floating Power Plant on the laboratory model.

Aalborg University, June 29, 2018

Contents

1 | Introduction

The present report is a part of the Danish EUDP project *"Mooring Solutions for Large Wave Energy Converter"*, and covers *Task 4.1: Creation/Acquisition of lab and real sea data for validation/calibration* and *Task 4.2 Pre-validation/calibration of Selected Tools for Full Dynamic Analysis*. The report, therefore, concludes *Milestone 5: Report on Validation/Calibration of Analysis Tools*.

The report summarizes the experimental campaign conducted in the wave basin at Aalborg University, investigating a simplified model of the Floating Power Plant. The experimental work was performed by Jonas Bjerg Thomsen, Francesco Ferri and a master student, Eduardo Calderón Asensio. Jens Peter Kofoed assisted in defining test plan and objective while Sarah Thomas from Floating Power Plant provided information on model layout and objective.

The report is structured with a chapter providing relevant information on the test set-up, procedure and preliminary results and is followed by a description of the numerical models, before comparison of results.

The report validates the use of both a quasi-static approach applied by many wave energy converter (WEC) developers [1], but also a full dynamic analysis tool selected based on the assessments in [2, 3]. The experimental work and validation in this report has also formed the basis for the papers [4] and [5], and the results are discussed in [6].

1.1 Objective of Experimental Tests

The test campaign was structured to provide data for validation of numerical tools to be used in future full dynamic analysis of the mooring systems for four large floating WECs. The tests are not intended to provide any optimal mooring solution, minimizing loads or motions, but merely to provide data for validation. Therefore, the mooring system used in the tests has not been optimized beforehand. The tools identified in this report are later used in [7] to optimize the mooring layout.

2 | Physical Tests

In order to validate the numerical models, a set of data was acquired through laboratory experiments. A two month test campaign was carried out in The Hydraulic and Coastal Engineering Laboratory, Aalborg University, Denmark, in the period from December 2015 to January 2016. The current chapter will describe the experimental set-up and the initial test results, while the following chapters will present the comparisons with numerical models. For more discussion of the test set-up, additional results and comparison see [4]. Unless other is specified, the report will present all result in full-scale values (1:64.5).

2.1 Experimental Test Set-Up

The experiments were conducted at the deep-water basin at Aalborg University, with a set-up as illustrated in Fig. 2.1. The investigated model was located 4.8 m in front of the wave maker, at a water depth of 0.7 m. Wave generation was controlled by the software package [8], and by use of a snake-type wave maker located at one end of the wave basin. A passive absorber (gravel beach) was located at the other end.

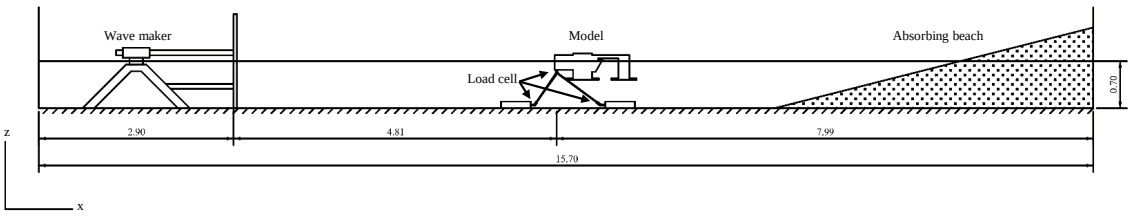

Fig. 2.1. Illustration of the test set-up. All measures are in [m].

For measuring of the generated surface elevation time series, a wave-gauge array was located approximately 1.5 m in front of the model, cf. Fig. 2.2. The array consisted of five resistant type wave gauges located in a 3D array, as shown in Fig. 2.2 and 2.3.

Acquisition of surface elevation measurements was handled by the software package [9], which was also used for analysis of reflection in the basin. Prior to the actual test campaign, all sea states were generated without the model in place in order to estimate the reflection arising from the basin geometry. The analysis proved insignificant wave reflection in the y-axis, and a maximum reflection coefficient of 0.2 in the x-axis for the longest waves. This was considered to be acceptable for the present tests.

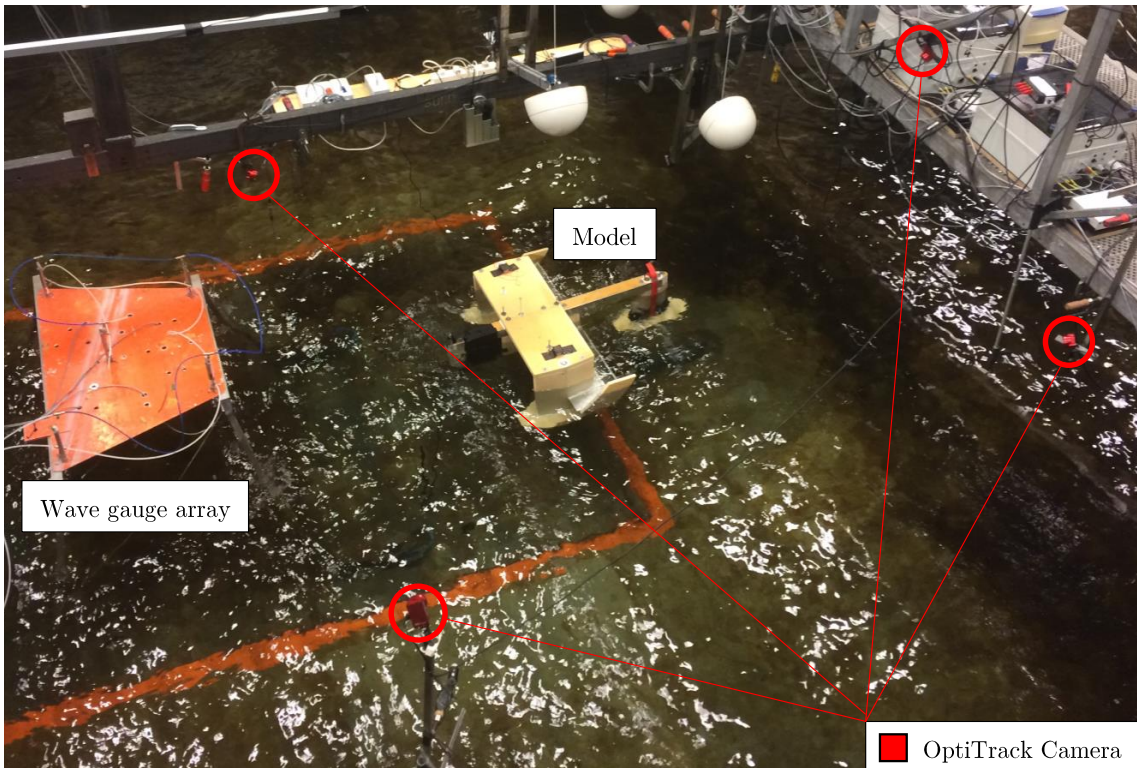

Fig. 2.2. Figure of test set-up with notation of wave gauge array, model and motion tracking cameras.

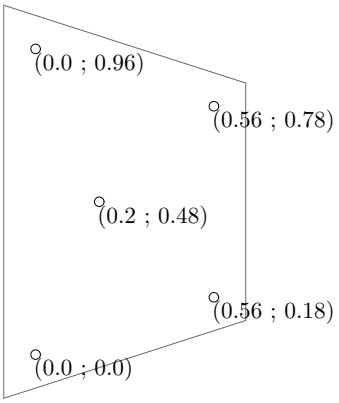

Fig. 2.3. Illustration of used wave gauge array with definition of coordinates for each gauge according to the local coordinate system.

The motion response of the model was measured using the motion tracking system OptiTrack [10] with four OptiTrack Flex 13 cameras (cf. Fig. 2.2) and five reflective markers (cf. Fig. 2.7). Data acquisition and analysis was performed using the Motive 1.9.0 software package.

Mooring loads were measured using four loadcells (cf. Fig. 2.4); Three *FUTEK LSB210 50/100 lb* load cells located at the anchoring points of the mooring lines, and one *VETEK 30 kg IP68* at the fairlead between lines and device (cf. Fig. 2.9). The data was acquired using WaveLab [9].

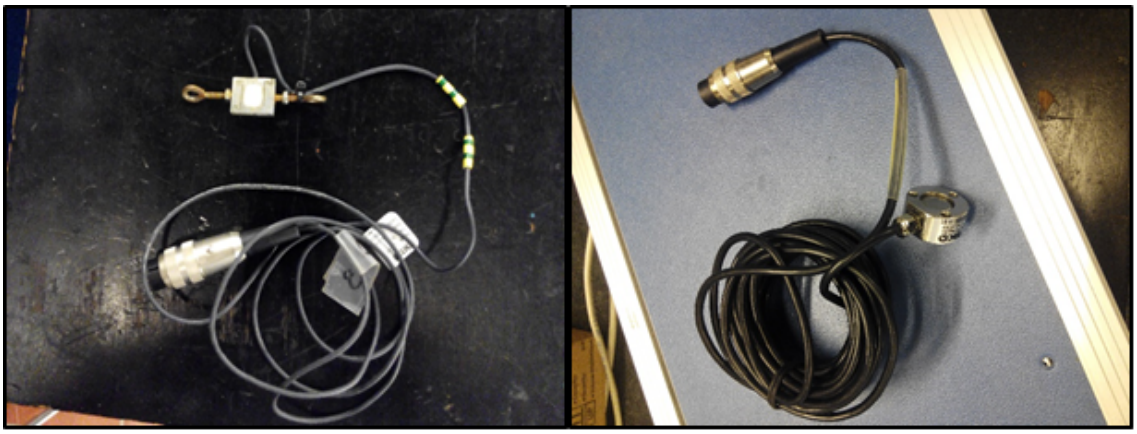

Fig. 2.4. Left: *FUTEK LSB210 50/100 lb* and right: *VETEK 30 kg IP68.*

2.1.1 Test Programme and Procedure

The test programme was planned in order to provide investigation of response in relevant operational and extreme sea states for the Floating Power Plant P60. A number of three operational and six extreme conditions were tested, together with 23 regular wave trains. The irregular sea states were simulated as JONSWAP spectra with a peak enhancement factor $\gamma = 3.3$. For information on the site conditions for the P60, see [11]. The water depth in the basin was 0.7 m, corresponding to 45.2 m in full scale (scale 1:64.5). In Fig. 2.5, the desired and acquired sea states are shown.

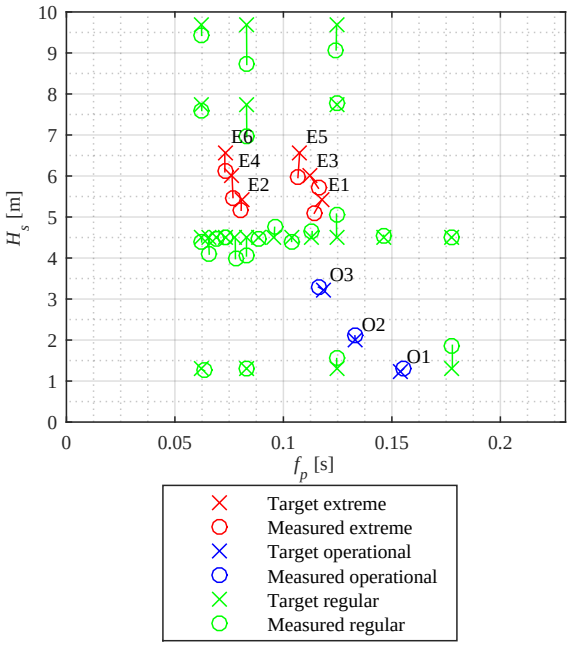

Fig. 2.5. Investigated sea states in the test campaign. E indicates an extreme sea state, while O indicates an operational.

Fig. 2.5 shows that good agreement was found between the target and measured peak periods and with minor difference between the significant wave heights. A maximum difference of 9% was found between target and measured wave heights, which is considered to be acceptable. The main objective of the test is to cover a range of wave frequencies expected at the site, and this is still obtained, hence, the difference is accepted.

2.1.2 Model

The model resembled a simplified geometry of the P60 device. In order to decrease the complexity of the model and tests, it was decided to remove the wind turbine and instead apply the mass at the base structure. Similarly, it was decided to remove the floaters and, hence, the model was constructed as shown in Fig. 2.6. Considering the objective of validating a numerical model, it is most important to ensure similarity between model and laboratory, and simplifying the model does not affect this, as long as the simplifications are similar in the numerical and experimental models.

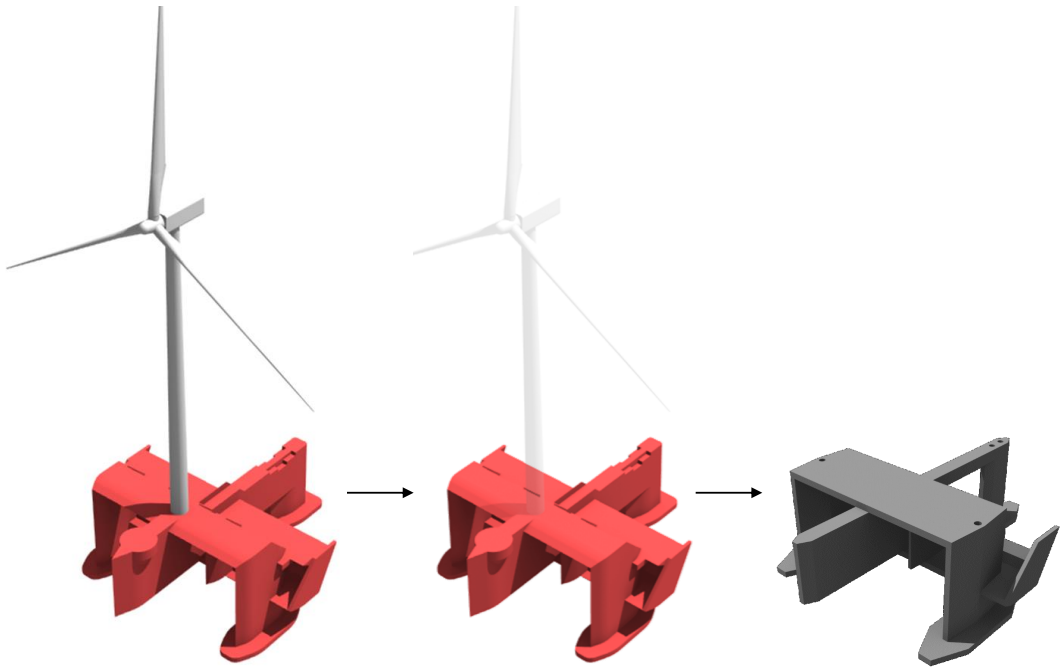

Fig. 2.6. Simplification of the P60 in the experimental model.

The base structure was build in high density foam, allowing for a strong and still light model, cf. Fig. 2.7. In order to obtain the desired total mass of the structure, additional mass was added to the structure. This allowed for different mass distributions, and investigation on its influence on response and mooring loads. For more information cf. [4].

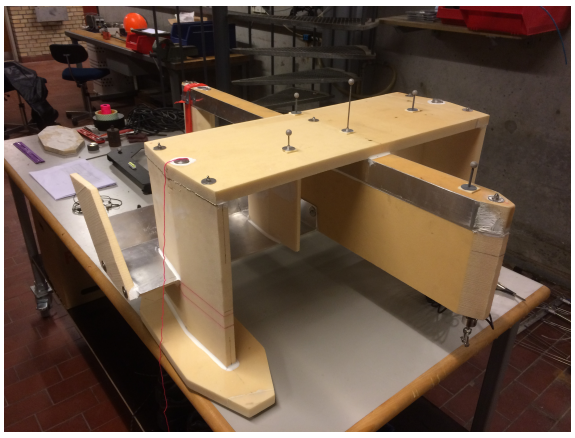

Fig. 2.7. Picture of the produced model used in the experimental tests.

The mass properties of the model were partly measured in the the laboratory and calculated using CAD software. The results are shown in Table 2.1.

	Unit	Value
Centre of gravity (x,y,z)	[m]	(32.9, 0.0, -4.8)
Mass	[kg]	$6.01 \cdot 10^6$
Mass moment of inertia, I_{xx}	[m^{2}kg]	$1.645 \cdot 10^9$
Mass moment of inertia, I_{yy}	[m^{2}kg]	$2.819 \cdot 10^9$
Mass moment of inertia, I_{zz}	[m^{2}kg]	$3.712 \cdot 10^9$

Table 2.1. Mass properties of the model in full-scale. Note that the MoI is around the centre of gravity.

2.1.3 Mooring Lines

Initially, the mooring solution applied to the P60 consisted of three mooring chains, but recent research in [12], showed the high potential benefit of applying synthetic ropes. This allowed for more compliance, lower tension and significantly less material and, therefore, also lower cost of mooring. As a result, very elastic, non-linear materials were used in the experiments. The measured stiffness of the lines are plotted in Fig. 2.8. Additional line properties are listed in Table 2.2. It is seen how the line stiffness of the low-stiffness line is approximately 60% of the stiffness of the basis case.

	Unit	Basis Case	Low k
Unstretched length	[m]	46.12	45.47
Stiffness	[-]	Cf. Fig. 2.8	
Linearized stiffness, EA	[MN]	11.54	4.69

Table 2.2. Line properties measured in the laboratory.

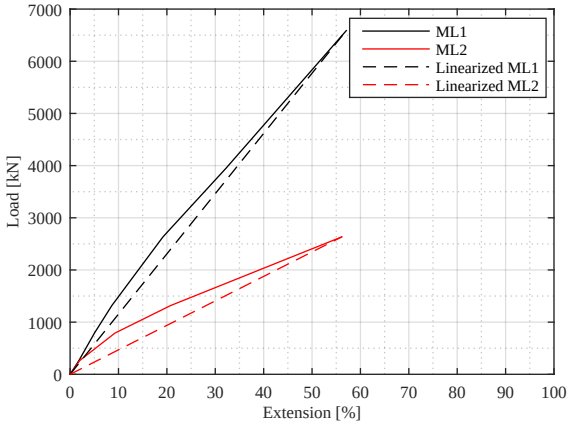

Fig. 2.8. Illustration of the measured tension-elongation curve for the two types of mooring line. ML1 corresponds to the basis case and ML2 corresponds to low k.

The test campaign does not aim to find the optimal mooring solution but merely to investigate the numerical models capability of modelling the response. The mooring system is, therefore, not optimized to the given sea states prior to the testing. It is, therefore, expected that a more optimal solution can later be found using the numerical tool, cf. [7].

The used mooring system consisted of three mooring lines as shown in Fig. 2.9. The lines were spread equally apart with 120° between them and with an initial stretching providing some pretension into the system. The mooring layout is shown in Fig. 2.9.

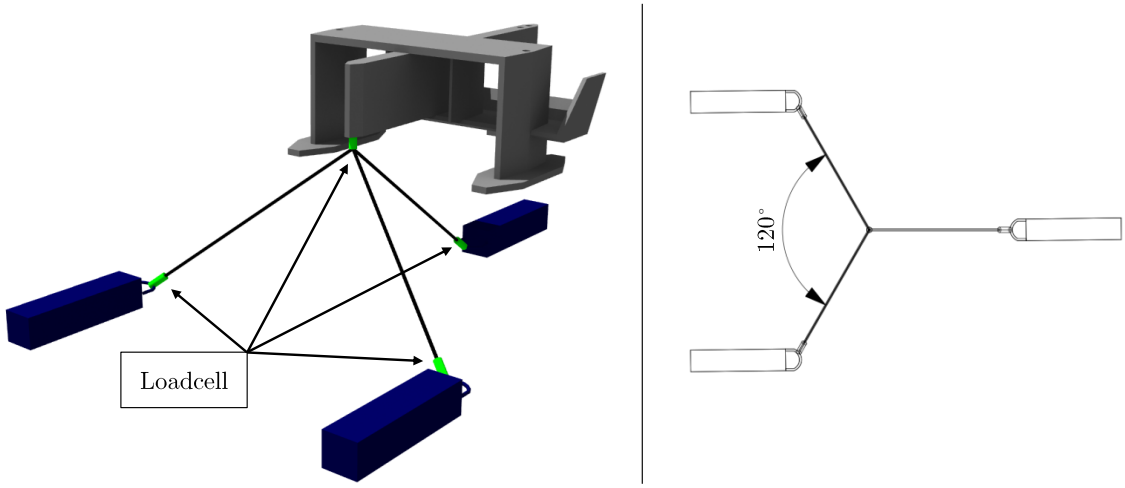

Fig. 2.9. Illustration of the mooring set-up with notation of load cells.

2.1.4 Quasi-static Test

The static stiffness of the system was determined by a quasi-static test, where the model was displaced at a low velocity. The displacement was limited to only the surge DOF. In doing so, the only restoring force in the system was a result of the mooring lines. The tensions measured during the quasi-static test is shown in Fig. 2.10.

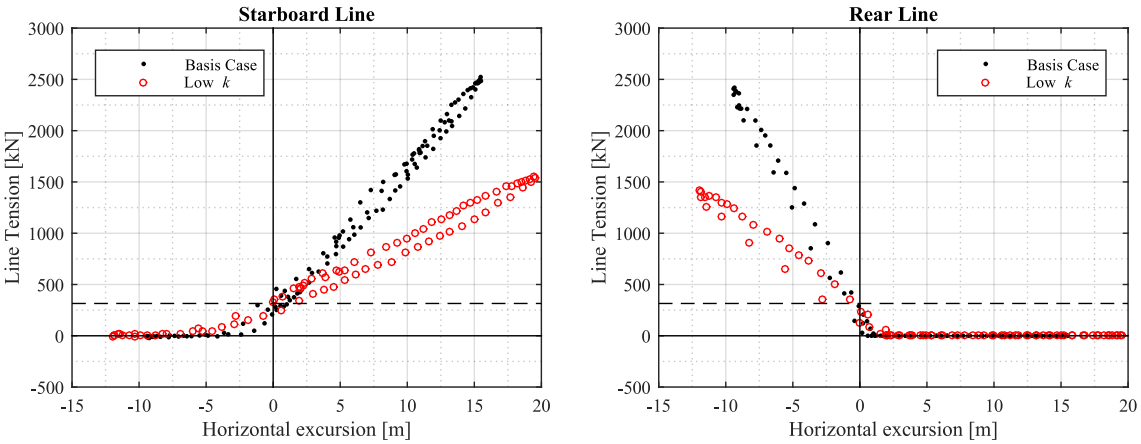

Fig. 2.10. Results from quasi-static tests of the two mooring configurations.

2.1.5 Natural Frequencies

In order to evaluate natural frequencies of the system, free decay tests were conducted. Here the model was given a static displacement in one DOF and released. The model was allowed to decay naturally, and the frequencies were determined from the response. Due to the complexity of the model and mooring application, activating only one DOF was a complicated task. Fig. 2.11 illustrates a test where each DoF was activated successfully, and allowed to decay. In most cases, however, a clear coupling between the DOFs was observed.

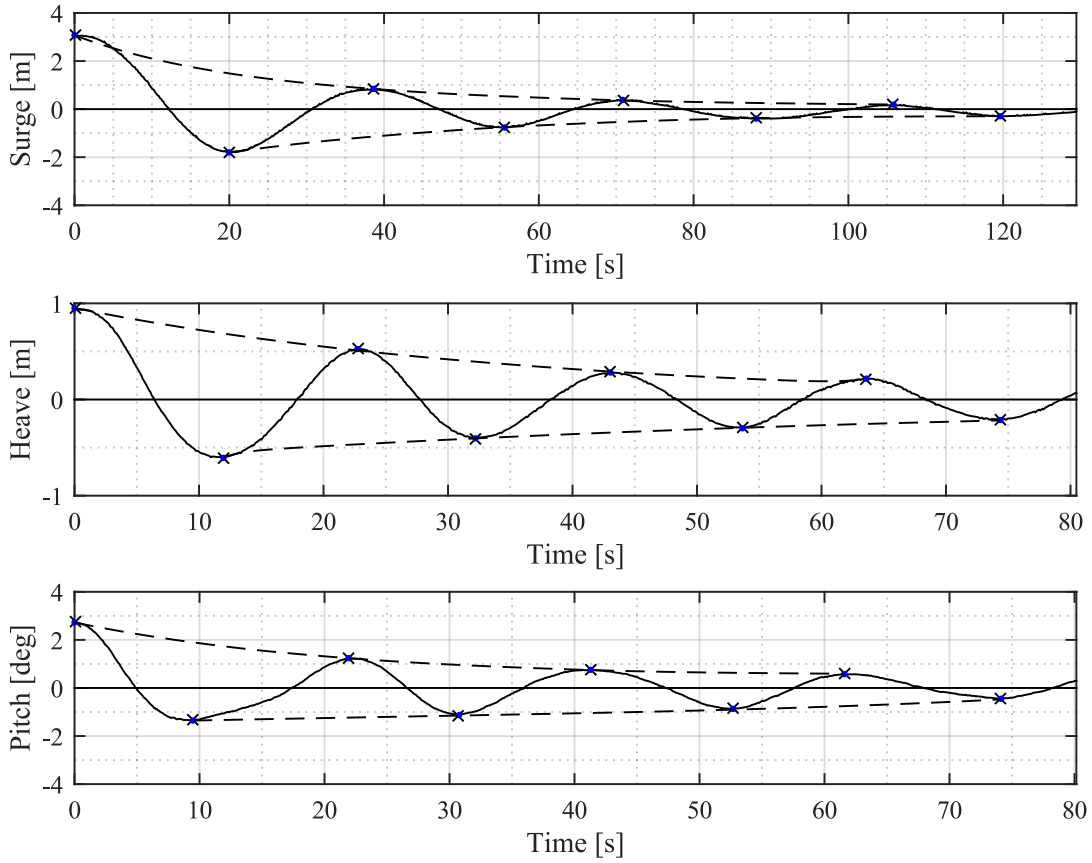

Fig. 2.11. Time series of the free decay tests. Adapted from [4].

Table 2.3 presents the measured natural frequencies for the two configurations. The values are determined from the decay tests (cf. Fig. 2.11) and the time distance in peaks and troughs. The presented values are average values. In addition to the natural frequencies, a coupled frequency was also observed at 0.078 Hz at which all DoFs were activated.

	Natural Frequency		
Case	**Surge**	**Heave**	**Heave**
Basis	0.0305	0.048	0.047
Low k	0.022	0.048	0.046

Table 2.3. Experimentally determined natural frequencies for the two investigated configurations.

2.1.6 Dynamic Response

The above parameters are useful in the description of the mooring and device, while the following sections describe the dynamic response, which are required in the design, evaluation and certification of the system. First, the motion response is presented, followed by a presentation of the mooring line tension response. These parameters are particularly used in the following chapters to validate the numerical tools.

Motions

Due to the present 2D problem, only the motion response in surge, heave and pitch is presented. Sway, roll and yaw were either non-present in the tests or restrained. Fig. 2.12 presents the response amplitude operators (RAOs) for the three DoFs for the two configurations.

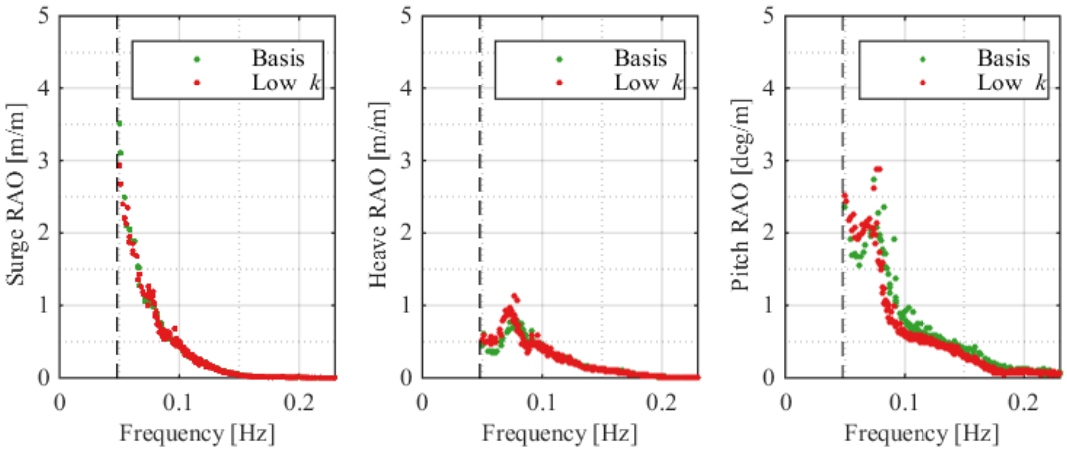

Fig. 2.12. Motion RAOs for the two investigated configurations.

Relatively good agreement between the two configurations are observed, despite the lower mooring stiffness in one of them. For the pitch DoF, the system with low stiffness is observed to have a slightly lower peak frequency, which is similarly observed for the heave DoF. Furthermore, it can be seen that the peak value is slightly higher for the low stiffness configuration. It is not possible to detect the peak in the surge DoF, due to the low natural frequency, cf. Table 2.3.

Tensions

The measured maximum tensions are presented in Fig. 2.13. Since the generated waves in each sea state are stored and rerun for each configuration, the wave time series are similar and a direct comparison between maximums are possible. It is clear that the maximum values are found in the basis case where the mooring lines are stiffer. This tendency was clearly expected, but it is paramount to note that a decrease of close to 50% can be achieved in the extreme cases from a 60% decrease of mooring line stiffness. This clearly underlines the potential of synthetic lines, particularly nylon, which is approximately twice as compliant as polyester.

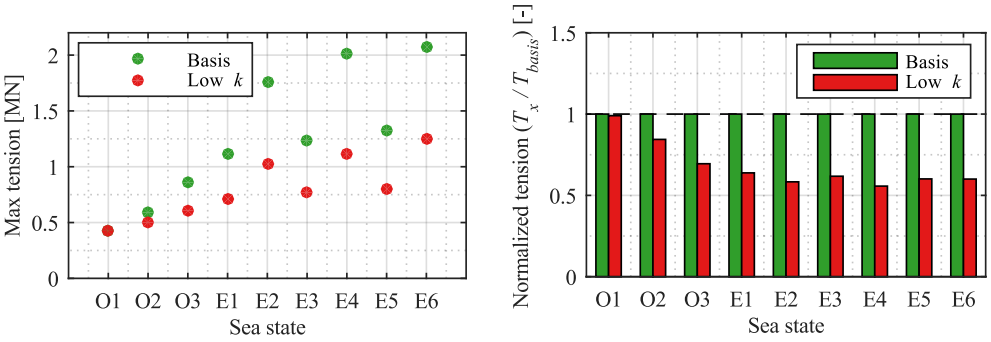

Fig. 2.13. Left: Presentation of measured maximum tensions in the front starboard line. Right: Comparison between the two configurations.

In addition to providing valuable information of the structure natural frequencies, expected motions and tensions, the experimental campaign provides a significant database of measurements that can be used to validate the numerical tools. The following chapters treat this matter.

3 | Hydrodynamic Model

When simulating the dynamic behaviour of the model under exposure of environmental loads, a numerical model is utilized, which can be divided into two components:

- A numerical model used to describe the wave-body interaction in the frequency domain. The BEM code Nemoh [13] is used.
- A numerical solver used to simulate the behaviour of the mooring lines and floating body under environmental exposure. The model can either be quasi-static or full dynamic and, furthermore, coupled, un-coupled, in frequency domain, or in the time domain, cf. e.g. [3]. This report presents a frequency dependent quasi-static un-coupled model, described in e.g. [14], and a commercial time domain dynamic software *OrcaFlex v10.0d* [15].

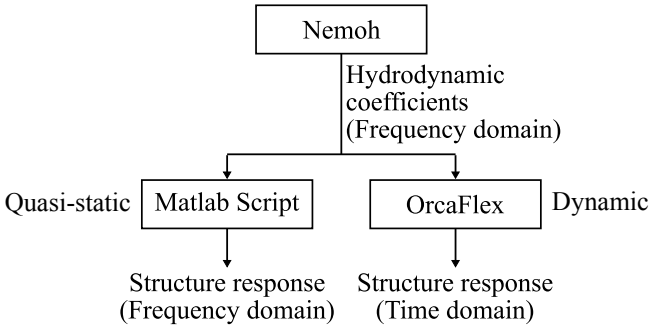

Fig. 3.1. Flow-chart of the numerical modelling procedures investigated in the present report.

This chapter describes the numerical models used for simulation of the investigated structure. The first section focuses on the wave-body interaction model, while the following section defines the used mooring parameters. The next two chapters will treat the quasi-static and dynamic models respectively.

3.1 Wave-Body Interaction Model

Loads on a floating structure at sea can be divided into a hydrostatic and a hydrodynamic part. When determining these load contributions, several methods/models can be implied. The most common includes Morison's Equations, the boundary element method (BEM) and computational fluid dynamics (CFD) with increasing computational demands. As a result of the very large computational cost of CFD simulations, often the Morison or BEM methods are considered. The Morison approach includes both a drag and an inertia term, while the BEM is based on diffraction and radiation. What model that is best suited is, therefore, dependent on the given case, and should be determined based on what load terms that are most dominating. Under some conditions it might be necessary to make

a hybrid model that includes all contributions. [16] developed the diagram illustrated in Fig. 3.2, which defines the force regimes in function of the Keulegan-Carpenter number and diffraction parameter.

When considering the sea states investigated in the present study (and plotted in Fig. 3.2), the main load contribution arises from the diffraction term. The cases are plotted by considering the structure as one solid structure, but considering Fig. 2.7, it is clear that water can flow through the model. Consequently, drag load contributions can be expected and need to be considered in the numerical model in order to achieve higher accuracy.

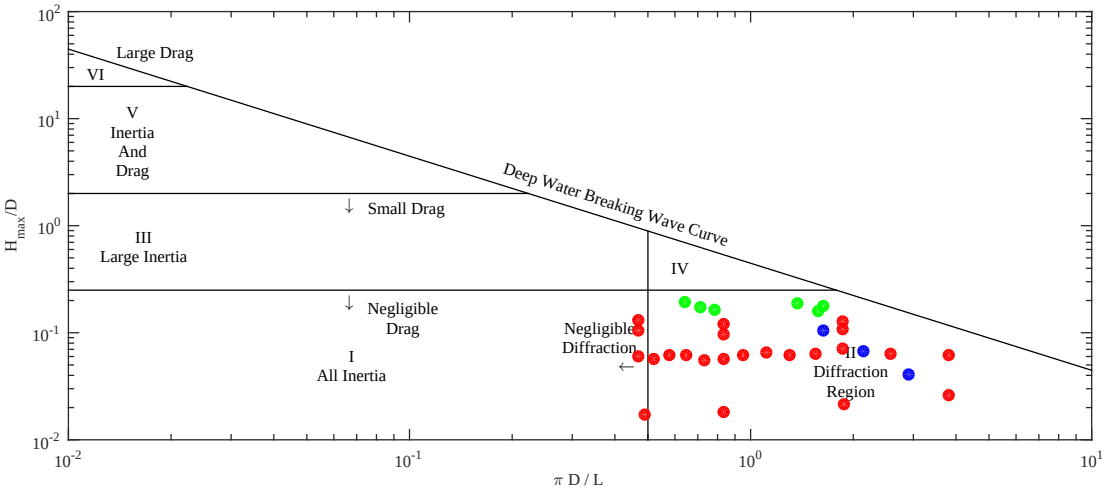

Fig. 3.2. Diagram used for determination of importance of the different load contributions on a floating body [16]. The x-axis describes the diffraction parameter, while the y-axis describes the Keulegan-Carpenter number (KC). Red markers indicate regular sea states, green indicated extremes and blue indicates operational.

3.2 BEM-method (NEMOH)

In the BEM, the Laplace equations are solved, invoking the assumptions of ideal fluid (inviscid, incompressible and irrotational). The hydrodynamic problem is solved for a 3D geometry and the velocity potential is solved for the fluid domain from the given boundary condition. Assuming small incident and radiated waves, the free surface boundary condition is linearised, and the loads acting on the body are approximated. The loads are separated into a radiation and excitation contribution.

The excitation contribution (F_{ex}) arises from the passing waves on the body held at the equilibrium position. The excitation force can be further divided into a Froude-Krylov and a diffraction contribution. The Froude-Krylov force (F_{KF}) is found from integration of the pressure on the body. Clearly, the oscillating nature of the pressure results in a oscillating Froude-Krylov force on the structure. It is assumed that the body does not disturb the wave field, but naturally the presence of the body results in diffraction of the waves, and hence, the Froude-Krylov force needs to be corrected. The diffraction contribution (F_{diff}) is therefore included, and the total excitation force can be found from (3.1).

$$F_{ex}(\omega) = F_{FK}(\omega) - F_{diff}(\omega) \tag{3.1}$$

The radiation force (B) arises from the oscillation of the body in still water. The motion of the body will induce waves propagating radially away from the body. The energy in these waves can be considered as a wave dissipation from the body motion,

hence the motion eventually dies out, and the contribution can be considered a damping, proportional to the motion velocity and introduced as a damping coefficient. The motion of the body additionally introduces a force contribution caused by the fact that the fluid particles close to the body needs to be accelerated along with it. This phenomenon is introduced as added mass (A) as it is in phase with the acceleration. The total radiation force (F_{rad}) can, therefore, be described by Eq. (3.2).

$$F_{rad}(\omega) = A(\omega)\ddot{x} + B(\omega)\dot{x} \tag{3.2}$$

Finally, the hydrostatic loads (F_{hyd}) can be defined as the load exerted by the fluid on the structure from the static pressure on the wetted surface. Without the presence of any dynamic behaviour, the only forces acting on the body is the gravitational and buoyancy forces. Archimedes' principle yields that the upward buoyancy force equals the weight of the volume displaced by the body. If assuming a small body, the hydrostatic load can be linearised as a restoring spring (K) force in function of the body displacement only. The force becomes:

$$F_{hyd} = Kx \tag{3.3}$$

The mentioned load contributions are calculated directly from the BEM (except the hydrostatic contribution) and can be used in the equation of motion to evaluate the structure response. Second order wave load contributions are not directly solved in the BEM, but can be evaluated from the first order quantities. Similarly, BEM does not account for the drag contributions and as mentioned, this need to be considered. In later sections, the two mentioned load contributions are described more detailed.

3.2.1 BEM Solver

The BEM solver used in this study is the open-sorce code Nemoh [13], which solves the hydrodynamic coefficients A, B and F_{ex} in the frequency domain. The software solves the pressure over the panels composing the submerged body. An example of a 3D model and the panel-mesh can be seen in Fig. 3.3.

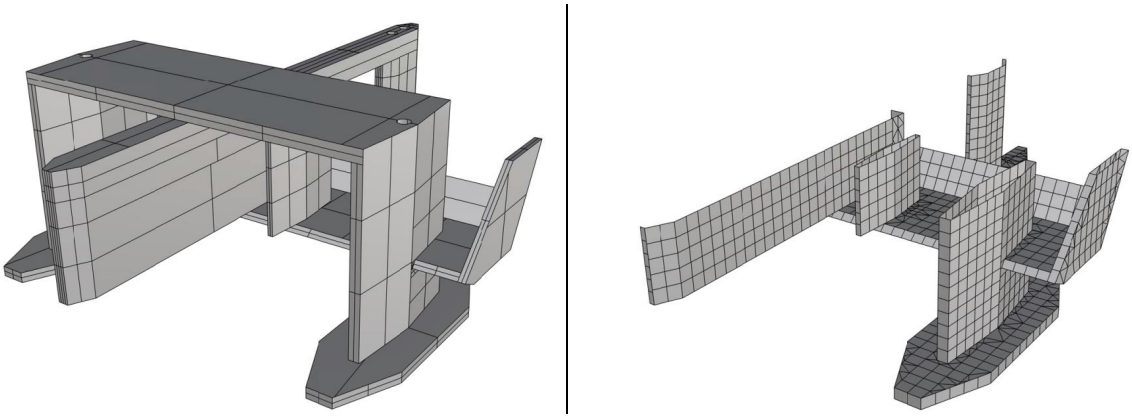

Fig. 3.3. Left: 3D model of the investigated structure. Right: Example of mesh used in the BEM code Nemoh. The mesh has a total number of 1768 panels.

3.2.2 Mesh Convergence Analysis for Floating Body

When constructing the mesh, the density of panels can be varied and potentially affect the results. Choosing a relatively small number of panels, n_p results in smaller computational

demands, but also a poorer description of the loads over the structure. Opposite, a larger number provides a better description of the loads, paid by the higher computational cost. A convergence analysis of the number of panels is, therefore, conducted, taking into account the excitation and radiation force (added mass and radiation damping). Figure 3.4-3.6, illustrates the calculated coefficients for different number of panels.

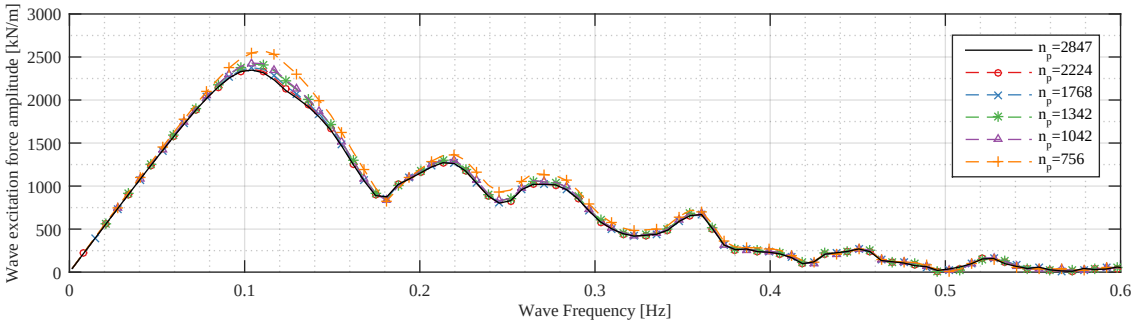

Fig. 3.4. Convergence analysis of wave excitation force coefficients.

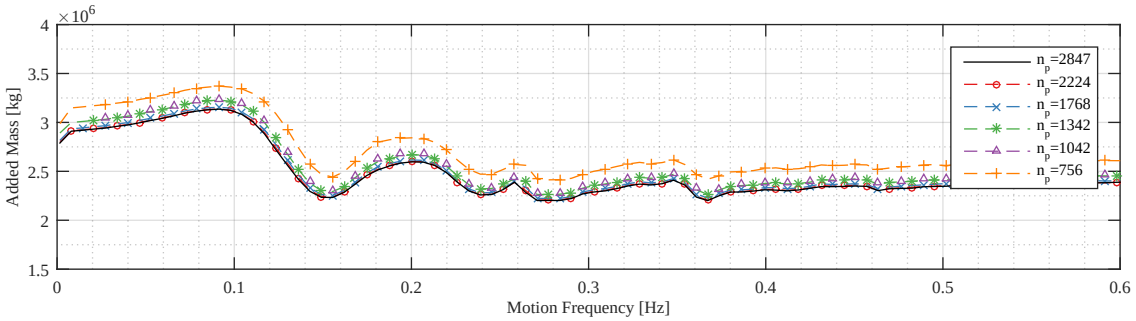

Fig. 3.5. Convergence analysis of added mass coefficients.

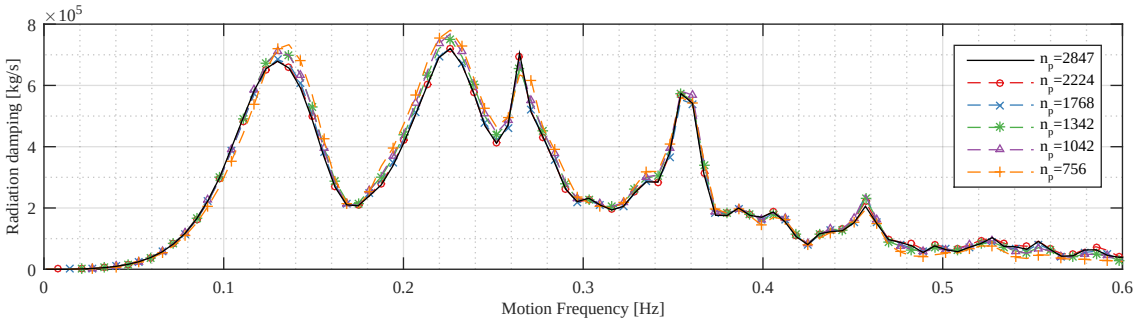

Fig. 3.6. Convergence analysis of radiation damping coefficients.

Fig. 3.7 illustrates the normalized error from the highly discretized mesh. A maximum error of approximately 10% was found for a mesh composed of 756 panels, while the error decreases to approximately 1% and below from 1768 panels. Based on this, a number of 1768 panels was selected for this analysis.

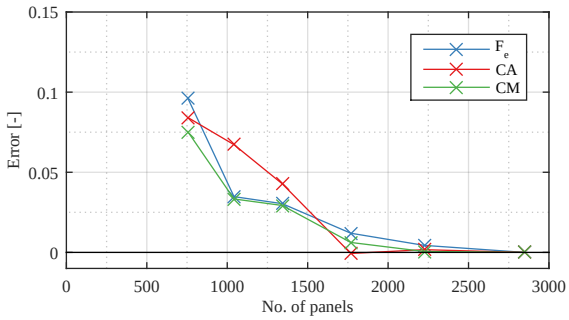

Fig. 3.7. Relative error for hydrodynamic coefficients for increasing number of mesh panels. The error is in relation to the results from the highest number of panels.

Even though convergence analysis is a valuable tool in ensuring high accuracy of the model, the computational demand is not as important as the accuracy. For a given structure, the BEM solver only needs to be run once, after which the results are input in the time/frequency solver, where environmental parameters etc. can be varied without influence from the number of panels on the body. Convergence analysis on e.g. mooring line discretization, therefore, becomes more important in order to limit computational time.

3.3 Second Order Slowly-varying Forces

The second order slowly-varying load can be described by QTF functions (Quadratic Transfer Functions), which tends to become time-consuming and more demanding to determine. In many cases, it is sufficient to utilize the Newman approximation [17], which uses the horizontal drift force coefficients to estimate the second order response. These coefficients can be evaluated from the first order quantities (e.g. found in Nemoh) using i.a. the far-field formulation by [18]. The approximation is valid in deep-water conditions and when the natural frequency of the systems is outside the investigated sea spectrum [19]. The latter will be valid in most cases when considering compliant moorings and extreme waves, while the first induces some uncertainties in the calculations.

3.4 Morison's Drag Load

Considering Fig. 3.2 it is seen that for long waves, the drag loads tends to become considerable in the total wave load. The linear BEM model does not take this load contribution into account. Often the Morison' equation is used to asses this load [20]. The drag load is calculated from the relative velocity of the structure, the body area and the drag coefficient, C_d. The latter can be calculated from higher order numerical models like CFD, or be determined from experimental tests. Drag coefficients for simple geometries can be found in literature [19, 21].

3.5 Results: Hydrodynamic and -Static Properties

In the following subsections, the hydrodynamic and -static properties calculated by Nemoh is defined.

The mass matrix is based on the measured values in the laboratory experiments, cf. Chapter 2, and is defined below.

$$M = \begin{bmatrix} 6.10 \cdot 10^6 \text{ kg} & 0 & 0 & 0 & 0 & 0 \\ 0 & 6.10 \cdot 10^6 \text{ kg} & 0 & 0 & 0 & 0 \\ 0 & 0 & 6.10 \cdot 10^6 \text{ kg} & 0 & 0 & 0 \\ 0 & 0 & 0 & 1.65 \cdot 10^9 \text{ m}^2 \text{ kg} & 0 & 0 \\ 0 & 0 & 0 & 0 & 2.82 \cdot 10^9 \text{ m}^2 \text{ kg} & 0 \\ 0 & 0 & 0 & 0 & 0 & 3.71 \cdot 10^9 \text{ m}^2 \text{ kg} \end{bmatrix}$$

3.5.1 Hydrostatic stiffness

The hydrostatic stiffness is calculated in the Centre of Gravity (CoG), based on the geometry of the mesh. The position does correspond to the equilibrium position with the applied mooring; hence, not a equilibrium position, when the mooring is not applied.

$$K_{hyd} = \begin{bmatrix} 0 & 0 & 0 & 0 & 0 & 0 \\ 0 & 0 & 0 & 0 & 0 & 0 \\ 0 & 0 & 3.19 \text{ kN/m} & 0 & 12.37 \text{ kN/rad} & 0 \\ 0 & 0 & 0 & 364.77 \text{ kNm/rad} & 0 & 0 \\ 0 & 0 & 12.37 \text{ kNm/m} & 0 & 661.86 \text{ kN/rad} & 0 \\ 0 & 0 & 0 & 0 & 0 & 0 \end{bmatrix} \cdot 10^3$$

3.5.2 Added Mass and Radiation Damping

When considering the added mass and damping calculated by Nemoh, only surge, heave and pitch are presented, since only waves approaching at 0° is considered.

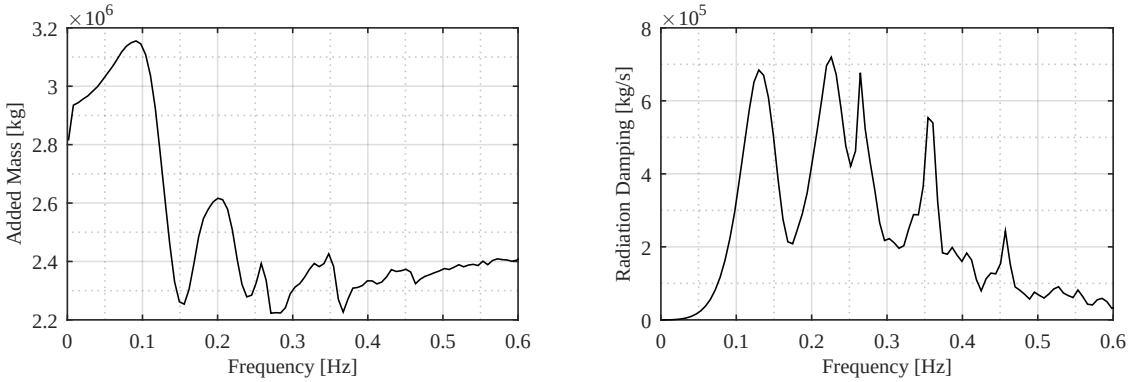

Fig. 3.8. Full-scale added mass and damping in the surge DoF.

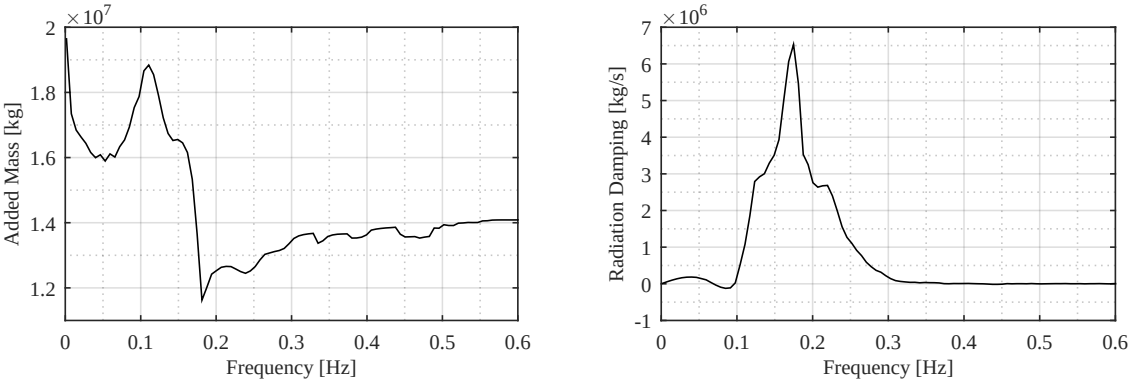

Fig. 3.9. Full-scale added mass and damping in the heave DoF.

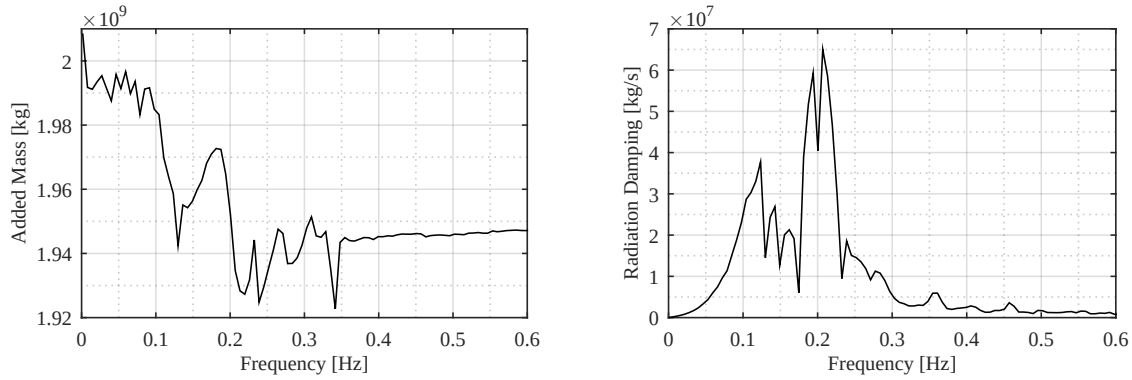

Fig. 3.10. Full-scale added mass and damping in the pitch DoF..

3.5.3 Excitation Force

Fig. 3.11- 3.13 present the excitation force amplitude and phase for respectively surge, heave and pitch.

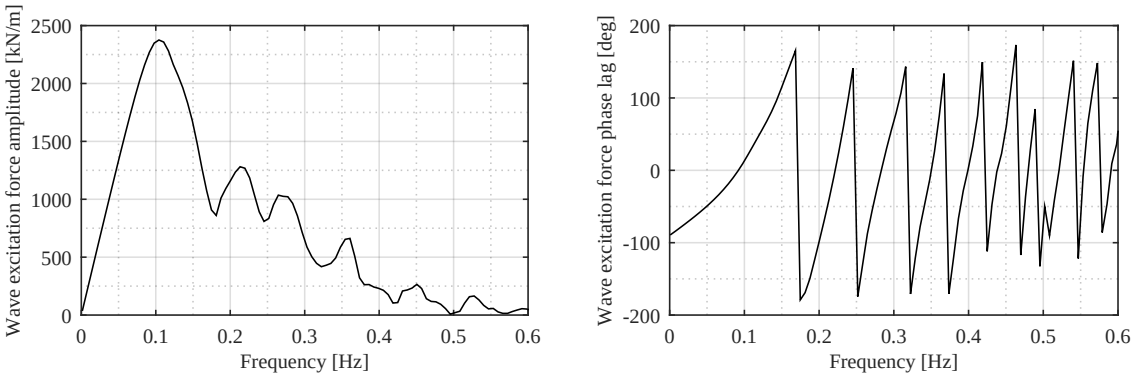

Fig. 3.11. Excitation force coefficients (Load RAOs) in surge.

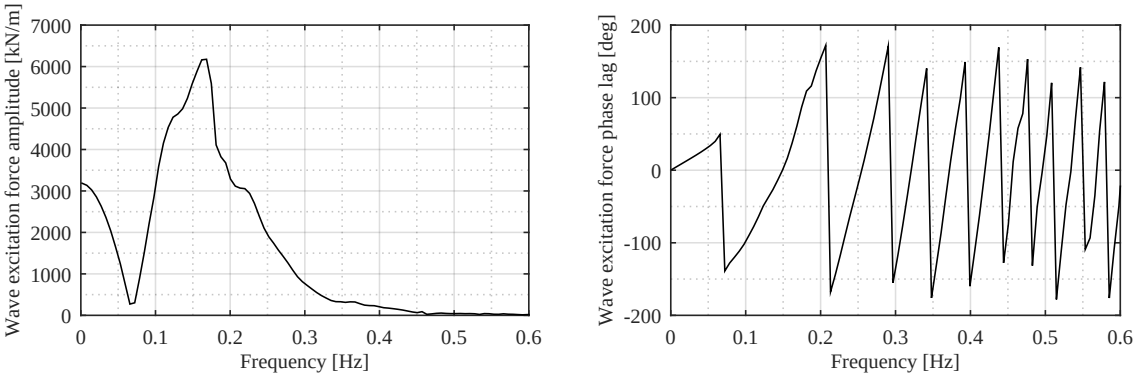

Fig. 3.12. Excitation force coefficients (Load RAOs) in heave.

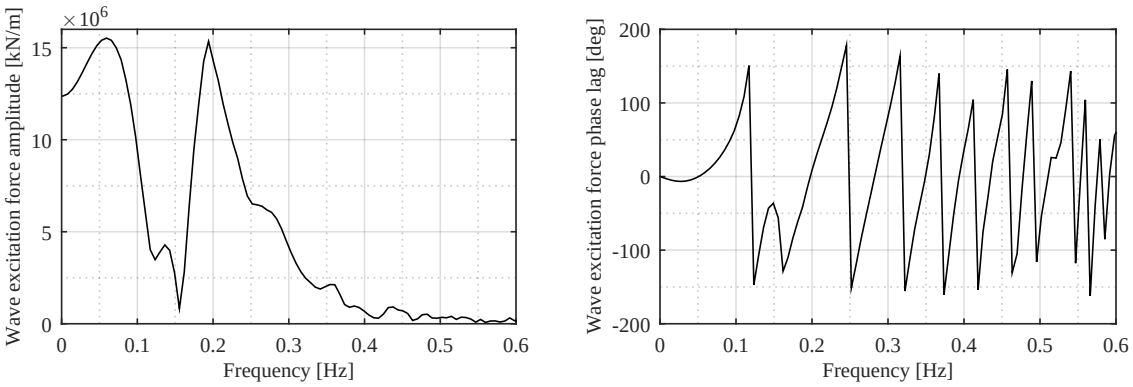

Fig. 3.13. Excitation force coefficients (Load RAOs) in pitch.

3.5.4 RAOs

Based on the equation of motion and the calculated hydrodynamic and static coefficients, the motion response amplitude operators (RAOs) can be calculated. These are presented in Fig. 3.14-3.16.

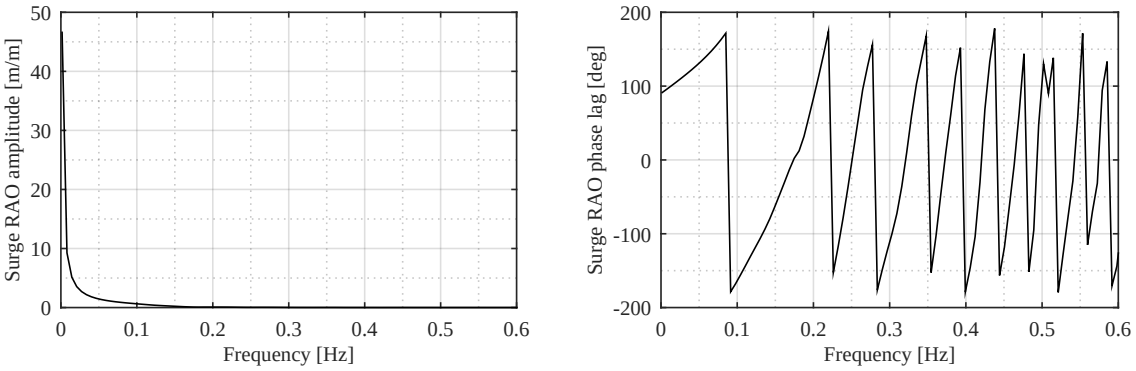

Fig. 3.14. Motion RAOs in surge DoF.

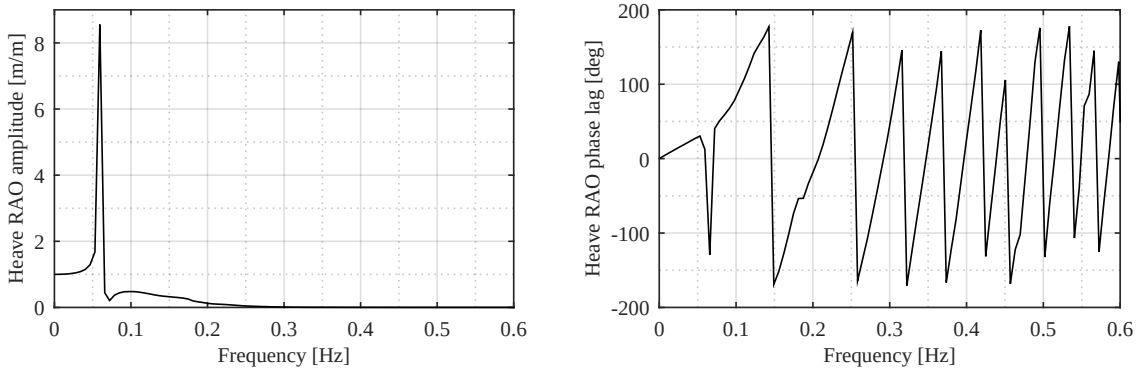

Fig. 3.15. Motion RAOs in heave DoF.

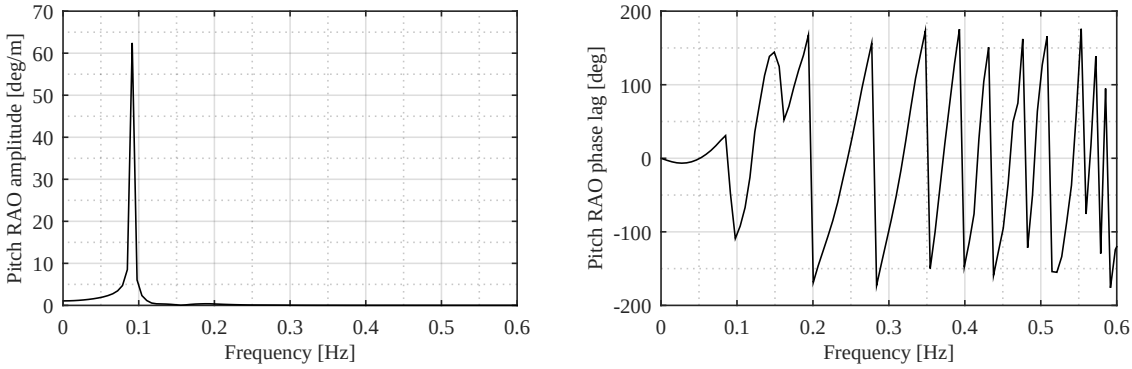

Fig. 3.16. Motion RAOs in pitch DoF.

3.5.5 Drift Force Coefficients

The drift force coefficient is calculated from the output of Nemoh using the methodology in [22].

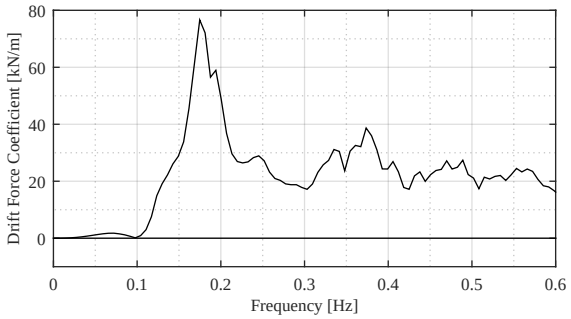

Fig. 3.17. Drift force in the surge DoF.

3.6 Mooring Line Properties

The numerical mooring model is defined in OrcaFlex, using up-scaled values of the experimental set-up. Anchor and fairlead positions are defined as:

Fairlead (x, y, z)	(0.00, 0.00, -11.93)
Anchor Starboard (x, y, z)	(-21.04, 36.44, -41.92)
Anchor Port (x,y,z)	(-21.04, -36.44, -41.92)
Anchor Rear (x,y,z)	(42.08, 0.00 -41.92)

The hydrodynamic properties of the lines are based on measured values and standard values found in [23]. The data is listed below.

Line diameter [m]	0.6
Bending Stiffness [kNm^2]	0
Drag coefficients (axial/normal)	0.0/1.6
Inertia coefficient (axial/normal)	0.0/1.0

4 | Quasi-Static Model

The quasi-static methodology for estimating the response of the moored WEC has been described in several publications such as [14], but also mentioned in design standards like [23] and [21]. Publications like [1] illustrated how many early stage WEC mooring designs have been based on this procedure and this chapter will adapt a similar approach (described in detail in [14]). The calculated design tensions will be compared to the experimental values. For more details on the calculations see also [4].

4.1 Modelling Procedure

The quasi-static analysis approach is illustrated in Fig. 4.1. The approach is based on a frequency domain analysis, and according to e.g. [21], consider only horizontal displacement (surge). As a consequence of the frequency domain approach, all non-linearities are linearized. For each line in the mooring system, a horizontal displacement-force curve is calculated and projected into the axis of the excursion in order to estimate the linear stiffness of the full mooring system. This stiffness is included in a 1-DoF spring-damper system, together with hydrostatic stiffness, mass properties and all hydrodynamic coefficients found using the BEM solver. Also second order motions are calculated from the drift coefficients. Solving the equations of motions, the response of the structure is determined, and the mooring loads can be found using the force-displacement curves.

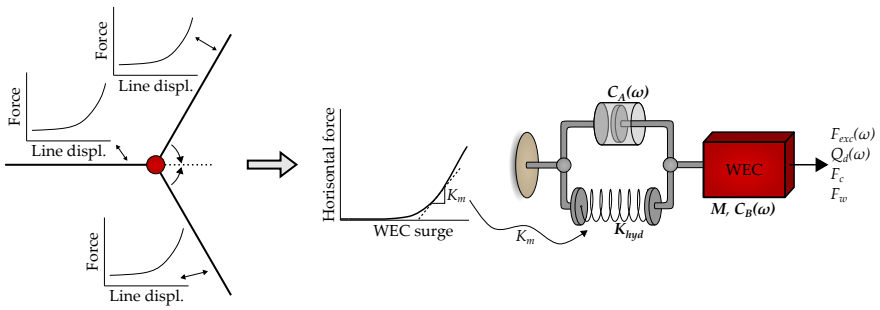

Fig. 4.1. Illustration of the modelling procedure in the quasi-static approach. Adapted from [6].

4.2 Validation of Quasi-Static Model

Fig. 4.2 presents the relative error between the calculated and measured tensions in the starboard line. The high frequency tests resemble the operational conditions and clearly represent the tests with lowest error. In these cases, the dynamic effects and non-linear influence from the mooring is least outspoken and the BEM code most reliable. For extreme sea states, the motions are highly underestimated and tensions likewise. For the

most extreme cases, underestimations of tensions of up to 50% are present. In a design case, this forms a considerable and critical error. More information is present in [4].

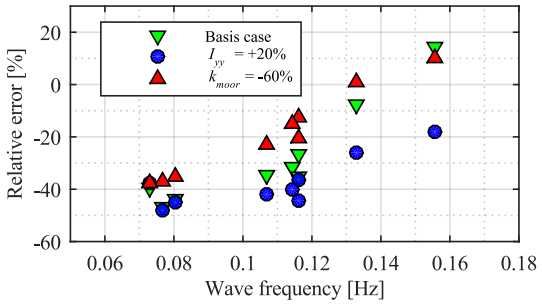

Fig. 4.2. Comparison between the experimentally measured tensions and tensions determined from the quasi-static analysis. The results from the three configurations presented in chapter 2 are all illustrated. Adapted from [6] and [4].

5 | Full Dynamic Analysis

The full dynamic analysis is based on the commercial software package OrcaFlex [15], and more detailed description can be found in [5]. The described procedure is e.g. utilized in [7].

5.1 Modelling Procedure

The moored WEC is modelled using a numerical model divided into two solvers. One, which solves the hydrodynamic interaction between WEC and waves, and one which solves the mooring line behaviour. The complete system can then be solves as a coupled system, where the mooring and WEC are solved simultaneously or as de-coupled where the WEC response is solves and the fairlead motions input in the mooring line solver and its response determined. The quasi-static approach follows the decoupled methodology, as the WEC response is solved with merely a mooring stiffness, and the motions are then used to determine tensions in the lines. The full dynamic model in this chapter considers a fully coupled system by use of the time domain solver OrcaFlex. Both the quasi-static and dynamic approach considered, use the hydrodynamic coefficient from Nemoh to describe the wave-structure interaction.

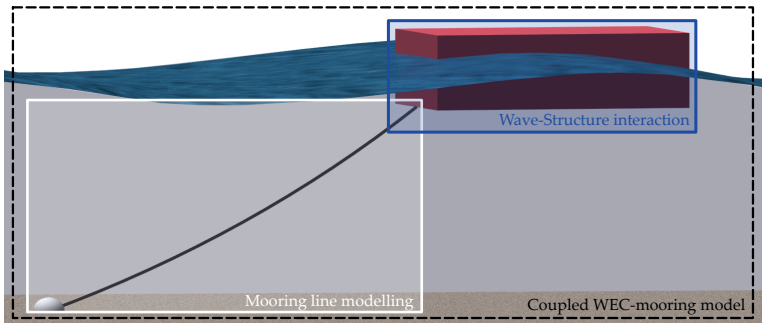

Fig. 5.1. Illustration of numerical models used in analysis of moored structures. Adapted from [6].

OrcaFlex utilizes the Cummin's Equation [24] to solve the time domain solution from the frequency domain parameters determined in Nemoh. The coefficients in this analysis allow for the determination of the force contributions from radiation and diffraction loads. Considering the diagram by [25] and [19] and plotted in Fig. 5.2, it is clear that when considering the structure as a closed volume, the diffraction/radiation loads are dominant. However, the structure is open and allows water to flow through it, thereby having a smaller characteristic diameter, D. Therefore, it becomes necessary to include load contributions from drag also, using Morison's Equation [20]. The present chapter illustrates the necessity of this by doing the analysis with and without drag elements in the model.

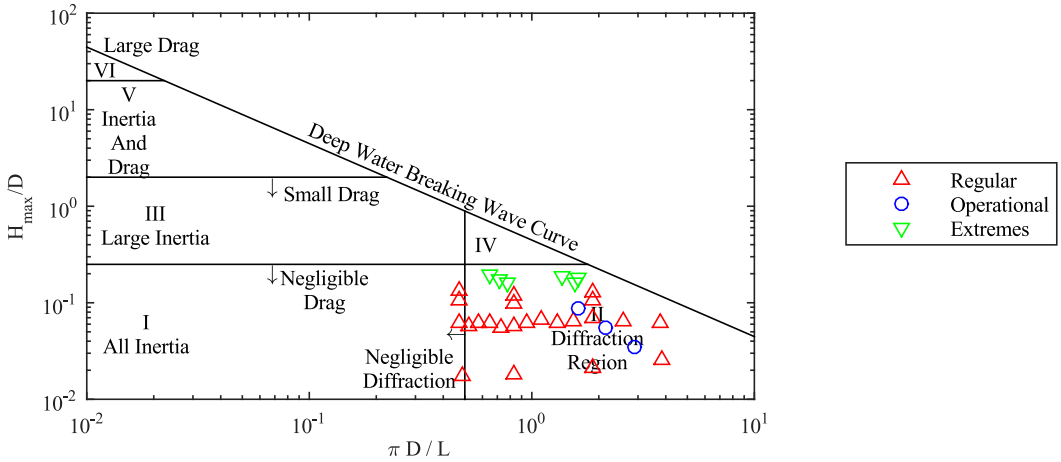

Fig. 5.2. Load regime as function of structure dimensions and incoming waves. Adapted from [5].

Morison's Equation requires a predefined drag coefficient, C_d, which needs to be determined using experimental methods or higher order numerical models like e.g. CFD. Many early stage WEC developers do not have access to this and, furthermore, the WECs often undergo many structural changes in the development phase. Consequently, it is necessary to estimate the coefficients using a simplified methodology, which does not require advanced methods and, therefore, can be utilized in all structures. By simplifying the model into simple shapes where values for C_d is known, it is possible to estimate combined coefficients for the structure. The simplified geometry is illustrated in Fig. 5.3 and the estimated values is presented in Table 5.1

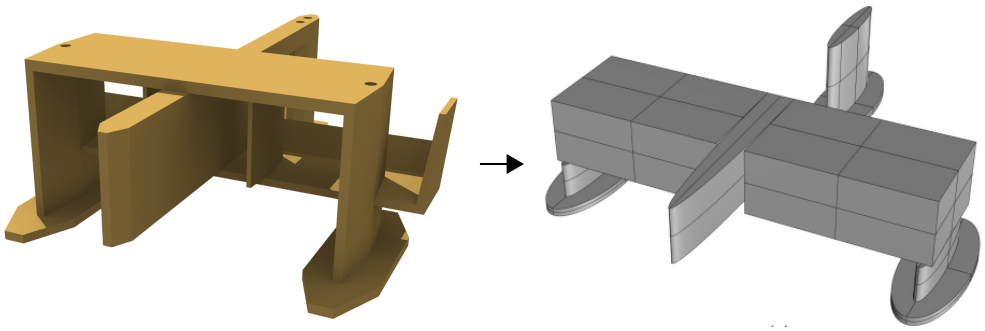

Fig. 5.3. Illustration of the simplified model geometry used to approximate drag coefficients. Adapted from [6].

Parameter	Surge	Heave	Pitch
Drag coefficient, C_d	1.35	1.68	1.25
Drag area, A_d	0.545×10^3 m^2	1.92×10^3 m^2	7.63×10^6 m^5

Table 5.1. Definition of drag coefficients and areas used in the numerical model.

OrcaFlex uses a lumped mass approach to calculate the mooring line response, where the lines are discretized into a number of elements, and masses etc. lumped to the nodes. For more details on this topic see [5, 6, 26, 27].

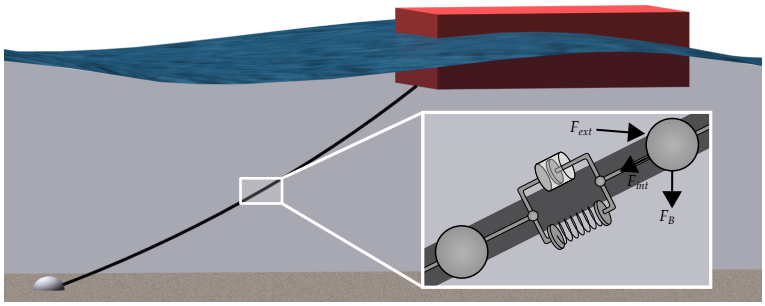

Fig. 5.4. Illustration of the test set-up. All measures are in [m].

Similar to the discretization of the panel mesh on the body, the number of elements in the lines, determines the accuracy of the results. Fig. 5.5 presents a convergence analysis of the line tensions in one mooring line. Clearly, the error is most visible in the minimum tension when the line is slacked. By dividing the lines into more than 15 elements, the error is less than 5% on the minimum value and less than 1% for the max.

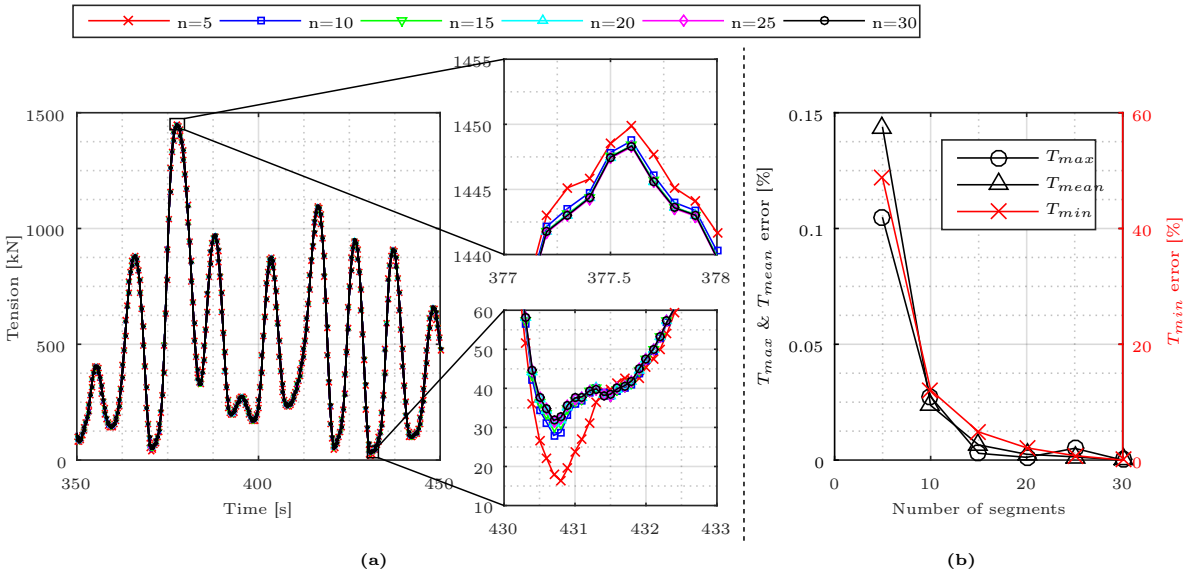

Fig. 5.5. (a) Time series of tensions for a different number of elements in the mooring line. (b) Error of each analysis compared to the case with maximum number of elements. Adapted from [5].

5.2 Validation

The experimental data acquired from the tests described in the previous chapter is used to validate the numerical model. It is important to note that the aim of the validation is to find a model, which can be used in initial design; hence, where some inaccuracies are acceptable. In final design, it is expected that more sophisticated models are needed in order to tune and calibrate the linear model in this report. For initial stages of mooring and WEC design, many changes are expected and finding an efficient model is required and this report tends to do so and evaluate potential deviations from experiments.

5.2.1 System Stiffness

The mooring layout and line tensions were initially validated through a quasi-static test, cf. Chapter 2. Fig. 5.6 presents the measured and calculated tension in the rear and starboard line. Due to the manual handling of the model in the experiments, some scattering is observed. However, the calculated tension is within this scatter, with the difference to some extent explainable by e.g. difference in the vertical displacement of the fairlead, cf. Fig. 5.6(c). Other differences are the presence of the loadcell in the experiments. The largest difference is seen in the slacked lines. It is evident that the numerical model estimates a tension even in slacked lines due to the buoyancy of the lines, while this is not observed in the experiments, possibly due to the loadcell. Still, the test illustrates good agreement between the model and experiment.

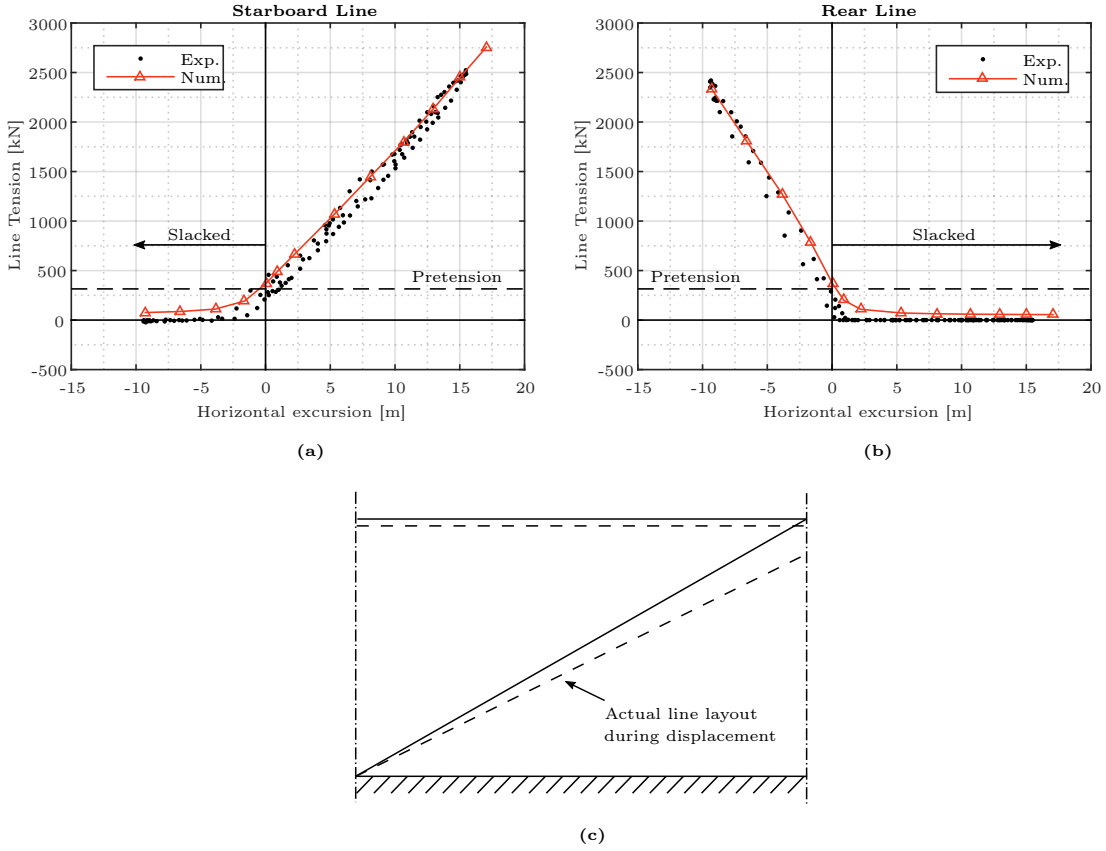

Fig. 5.6. Static test of the tension in starboard and rear mooring line. Adapted from [5].

5.2.2 Decay Tests

For validation of the natural frequencies, a decay test was performed. Due to a coupled frequency and the complex geometry, it was only possible to activate the surge DoF. When attempting to activate only heave and pitch, motions in all DoFs were observed. Fig. 5.7(a) presents a time series of surge decay.

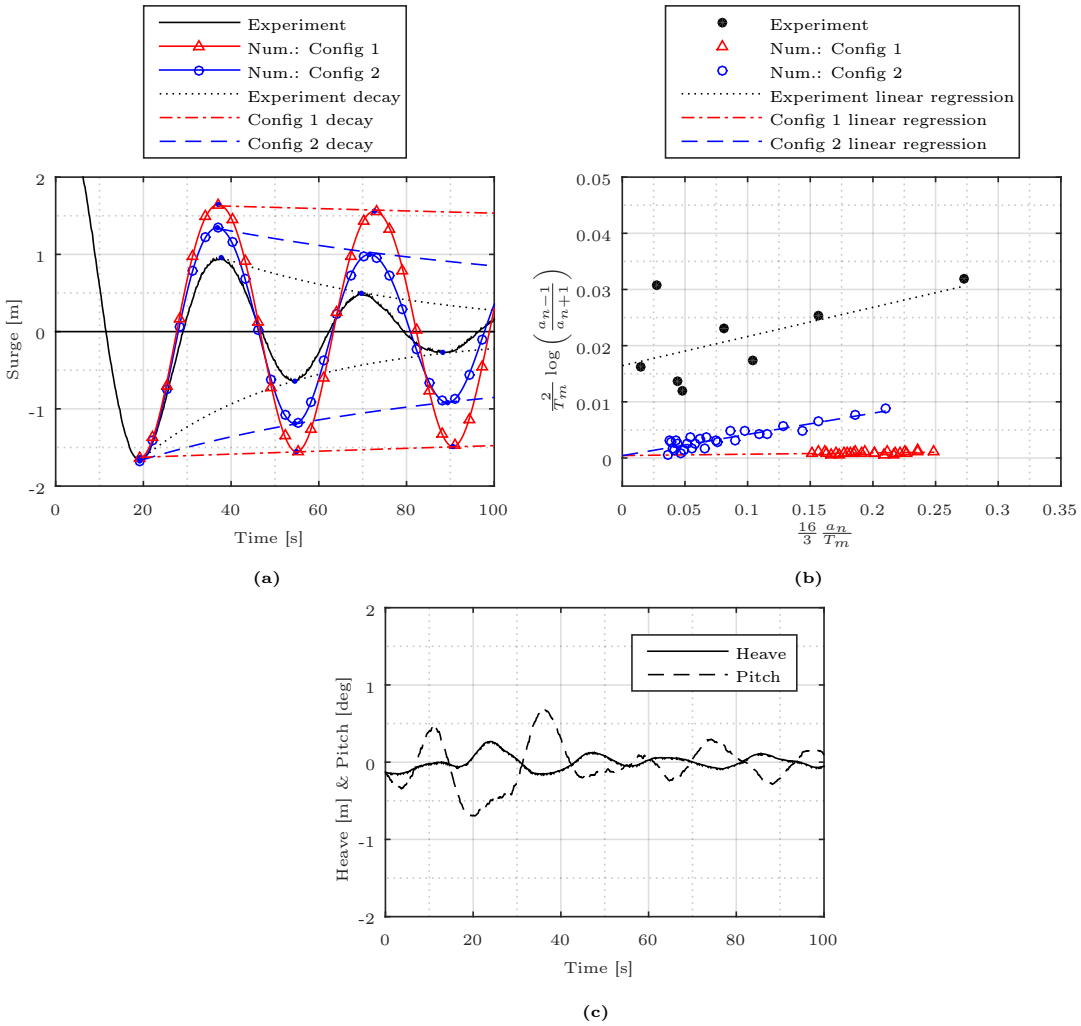

Fig. 5.7. Surge decay test (a), determination of damping (b) and heave and pitch motion during the surge decay test (c). Adapted from [5].

During the decay tests, the structure motions are dependent on the structure mass, added mass, radiation damping, hydrostatic stiffness and mooring stiffness. In the above test, the structure mass is similar in the numerical and experimental model, while no hydrostatic stiffness is present in surge. The mooring stiffness was shown in Fig. 5.6 to be reliable, for what reason the difference in the decay test is a result of inaccuracy in estimating the radiation damping and added mass. Table 5.2 present the values for natural frequency in the experiments and numerical model. The natural frequency is mostly dominated by the added mass and a relatively small error is observed.

	Experiment	Num.: Config 1 Value/Error	Num.: Config 2 Value/Error
Surge frequency, f_n	0.0305 Hz	0.0284 Hz / 6.9%	0.0293 Hz / 3.9%
Linear damping, p_1	0.0164 s^{-1}	0.0004 s^{-1} / 97.6%	0.0004 s^{-1} / 97.6%
Quadratic damping, p_2	0.0519 m^{-1}	0.0024 m^{-1} / 95.4%	0.0378 m^{-1} / 27.2%

Table 5.2. Measured and calculated natural frequency, linear and quadratic damping in surge, together with the relative error. Adapted from [5].

Using the methodology described in [19] and presented in [5], the linear and quadratic damping, p_1 and p_2, is evaluated from Fig. 5.7(c) and presented in Table 5.2. The effect of the drag term on the quadratic damping is evident when comparing Configuration 1 and 2 (respectively with and without drag), while it is clear that the numerical model is unable to accurately evaluate the linear damping.

5.2.3 Regular Wave Tests

As presented in Fig. 2.5, a number of regular sea states were tested in the laboratory and similarly in the numerical model. In Fig. 5.8, the motion response amplitude operators (RAOs) of the structure are compared. It is evident that absence of drag elements causes high inaccuracy at the peak frequency. For the test with drag element (Config 2), relatively good agreement is achieved.

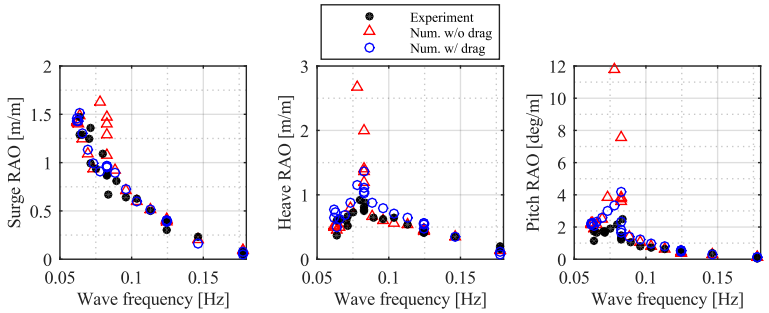

Fig. 5.8. Comparison of motion RAOs for the two configuration. Adapted from [6].

Fig. 5.9 presents the mean drift measured and calculated for the model. It is observed that the trends of the results are similar between the experimental and numerical, but the configuration without drag causes high inaccuracy around the motion peak values shown in Fig. 5.8.

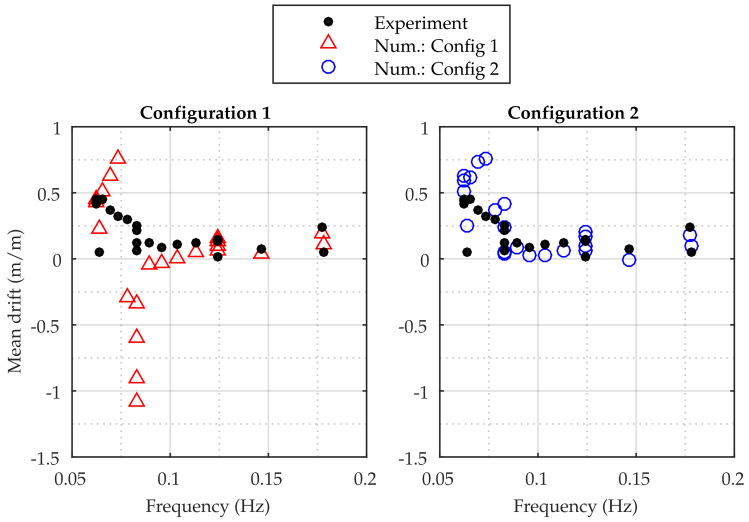

Fig. 5.9. Drift motion RAOs for the experimental and numerical model. Adapted from [5].

5.2.4 Irregular Wave Tests

A number of irregular wave tests were simulated and the most probable maximum tensions from the starboard line are compared in Fig. 5.10. For the operational sea states (high frequency), the influence of the drag element is without affect on the tensions, while it becomes crucial to include in the highly dynamic extreme seas. The model without drag was incapable of finding a solution in the extremes, as the response became so exaggerated, that the numerical solver became unstable. For the model with drag elements, the maximum relative error between measured and calculated tension is 11 %.

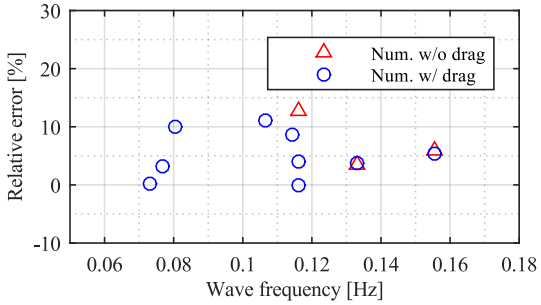

Fig. 5.10. Relative error between measured and calculated tensions in the starboard line. Adapted from [6].

5.2.5 Optimized Model Example

When considering the above sections, it is clear that a reasonable error is obtained by using the described simplified numerical model with coarse estimation of drag elements. A maximum numerical error of 11% can be accepted for initial designs, but must be reduced in final stages of the design in order to make the most realistic and accurate description of the structure and mooring response. At present, an overestimation of the tensions is achieved, which is acceptable from a safety point-of-view but undesirable when considering the cost. From Table 5.2, it is observed that the linear damping is highly underestimated in the present numerical model, possible due to numerical error in modelling the heaving plates. By adding linear damping through an iterative process, the results in Fig. 5.11

and 5.12 are achieved. Clearly, a much better description of the heave, surge and pitch motions are obtained, and similarly for the drift. Considering Fig. 5.11(a), it is now clear that the combined added linear damping, and quadratic damping from the drag element, is much closer to the measured damping. This is also observed from Fig. 5.11(b), where the linear and quadratic damping now resembles the measured.

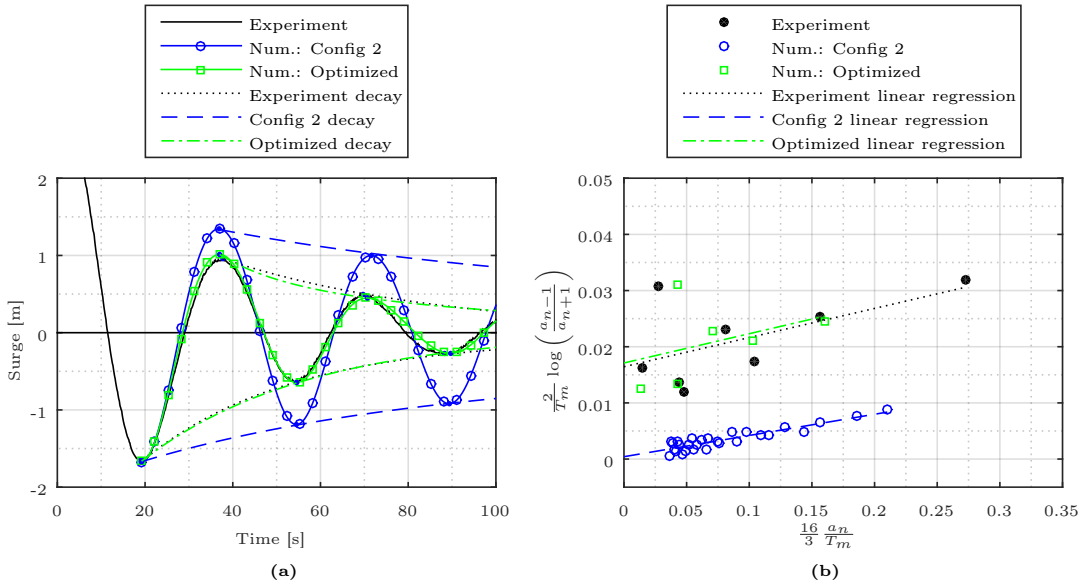

Fig. 5.11. Comparison between surge decay test from experimental and numerical model. The numerical model illustrates the configuration with a drag element only, and one optimized model with added linear damping. Adapted from [5].

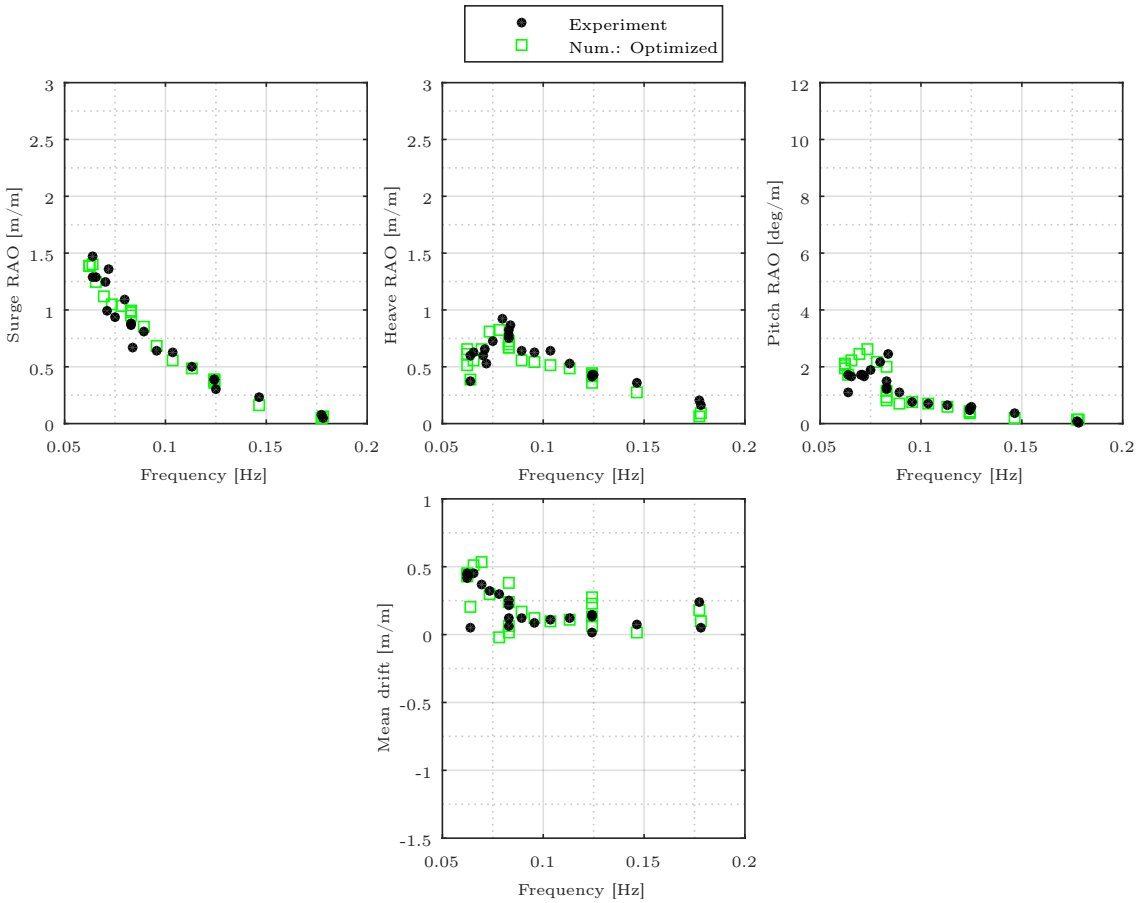

Fig. 5.12. Comparison between motion RAOs from experimental and optimized numerical model. Adapted from [5].

In order to achieve this optimized model, it is necessary to perform experimental tests or higher order numerical models. As described, this is necessary in final stages of the mooring design, while the method described in this report is sufficient in initial phases.

6 | Conclusion

The present report has described the experimental test campaign conducted at Aalborg University in December 2015 to January 2016. Similarly, a numerical hydrodynamic model was described to estimate wave-structure interaction, while both a quasi-static and full dynamic model for tension and motion response evaluation were described. The models were validated against the experimental data in order to find a model to be used further in the MSLWEC project for initial mooring design, and to provide general guidelines for such analysis. The experimental work illustrated the great benefit of using highly compliant lines in order to gain a significant reduction of mooring loads.

Fig. 6.1 presents the error in line tensions obtained in both the quasi-static and dynamic model. It is clear that at substantial difference is achieved between the two models. As expected and presented in other publications like [14], the quasi-static model provides a significantly larger error than the dynamic. It is critical that the use of quasi-static methods, which have been the case for many developers in early stages of the design [1], provides an underestimation of the tensions of up to 50% in the most extreme design cases. Use of the presented dynamic analysis reduces this error to a maximum of 11% and, more importantly, it is an overestimation of the loads, which is clearly more desirable in order to obtain high safety.

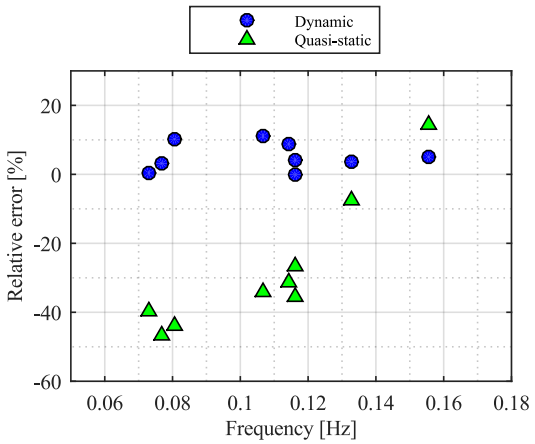

Fig. 6.1. Comparison between the tension error obtained between quasi-static and dynamic models and experimental data.

It is clear from Fig. 6.1 that the use of quasi-static approaches are insufficient in extreme cases, while the use of a dynamic model can be applied with some overestimation of the motions and loads. In a final design of the mooring system, it is still recommended to perform experiment or higher order numerical models in order to provide a better understanding of the response, to tune the linear model and to secure high cost efficiency and reliability.

References

[1] Jonas Bjerg Thomsen, Francesco Ferri, and Jens Peter Kofoed. Assessment of Current State of Mooring Design in the Danish Wave Energy Sector. In *Proceedings of the 11th European Wave and Tidal Energy Conference EWTEC2015*. Technical Committee of the European Wave and Tidal Energy Conference, 2015.

[2] Jonas Bjerg Thomsen, Claes Eskilsson, and Francesco Ferri. *Assessment of Available Numerical Tools for Dynamic Mooring Analysis: WP1.2 & M1.* Department of Civil Engineering, Aalborg University, 2017.

[3] Jonas Bjerg Thomsen, Francesco Ferri, and Jens Peter Kofoed. Screening of Available Tools for Dynamic Mooring Analysis of Wave Energy Converters. *Energies*, 10(7), 2017.

[4] Jonas Bjerg Thomsen, Francesco Ferri, and Jens Peter Kofoed. Experimental Testing of Moorings for Large Floating Wave Energy Converters. *Progress in Renewable Energies Offshore RENEW2016*, 2016.

[5] Jonas Bjerg Thomsen, Francesco Ferri, and Jens Peter Kofoed. Validation of a Tool for the Initial Dynamic Design of Mooring Systems for Large Floating Wave Energy Converters. *Journal of Marine Science and Engineering*, 5(4), 2017.

[6] Jonas Bjerg Thomsen. *Mooring Solutions for Large Wave Energy Converters.* PhD thesis, 2017.

[7] Jonas Bjerg Thomsen, Francesco Ferri, Jens Peter Kofoed, and Kevin Black. Cost Optimization of Mooring Solutions for Large Floating Wave Energy Converters. *Under review for publication in Energies*, 2017.

[8] AwaSys 7. Two and three dimensional wave generation, 2016. [Online]. Available: `http://www.hydrosoft.civil.aau.dk/awasys/`.

[9] WaveLab 3. *Data Acquisition and Analysis Software.* Department of Civil Engineering, Aalborg University, 2016. [Online]. Available: `http://www.hydrosoft.civil.aau.dk/wavelab/`.

[10] OptiTrack. *Motion Capture Systems.* NaturalPoint, Inc., 2016. [Online]. Available: `https://www.optitrack.com/`.

[11] Jonas Bjerg Thomsen, Francesco Ferri, and Jens Peter Kofoed. *Current Mooring Design in Partner WECs and Candidates for Preliminary Analysis: CM1 & M3.* Aalborg University, Department of Civil Engineering, 2016. Confidential report.

[12] Jonas Bjerg Thomsen, Jens Peter Kofoed, Martin Delaney, and Stephen Banfield. Initial Assessment of Mooring Solutions for Floating Wave Energy Converters.

In *The 26th International Ocean and Polar Engineering Conference ISOPE2016*. International Society of Offshore and Polar Engineers, 2016.

[13] Aurélien Babarit and Gérard Delhommeau. Theoretical and numerical aspects of the open source bem solver nemoh. In *11th European Wave and Tidal Energy Conference (EWTEC2015)*, 2015.

[14] Lars Bergdahl and Jens Peter Kofoed. *Simplified Design Procedures for Moorings of Wave-Energy Converters: Deliverable 2.2*. DCE Technical Reports. Department of Civil Engineering, Aalborg University, 2015.

[15] Orcina Ltd. *Orcaflex User Manual*. 2013.

[16] Subrata Kumar Chakrabarti. *Hydrodynamics of offshore structures*. WIT press, 1987.

[17] JN Newman. Second-order, slowly-varying forces on vessels in irregular waves. 1974.

[18] JN Newman. The drift force and moment on ships in waves. *J. Ship Res.*, 11(1):51–60, 1967.

[19] Odd Faltinsen. *Sea loads on ships and offshore structures*, volume 1. Cambridge university press, 1993.

[20] JR Morison, JW Johnson, SA Schaaf, et al. The force exerted by surface waves on piles. *Journal of Petroleum Technology*, 2(05):149–154, 1950.

[21] API. *Design and Analysis of Stationkeeping Systems for Floating Structures*. American Petroleum Institute API-RP-2SK, 2005.

[22] Jonas Bjerg Thomsen. *Validation of Mean Drift Forces Computed with the BEM Code NEMOH*. Department of Civil Engineering, Aalborg University, 6 2017.

[23] DNV-GL. *Position Mooring*. DNV-GL Offshore Standard DNVGL-OS-E301, 2015.

[24] WE Cummins. The impulse response function and ship motions. Technical report, David Taylor Model Basin Washington DC, 1962.

[25] Subrata Chakrabarti. *Handbook of Offshore Engineering*. Elsevier, 2005.

[26] Matthew Hall and Andrew Goupee. Validation of a lumped-mass mooring line model with deepcwind semisubmersible model test data. *Ocean Engineering*, 104:590–603, 2015.

[27] Josh Davidson and John V Ringwood. Mathematical Modelling of Mooring Systems for Wave Energy Converters—A Review. *Energies*, 10(5):666, 2017.

ISSN 1901-726X
DCE Technical Report No. 245